

# Estimation of roughness-induced scattering losses in III-nitride laser diodes with a photoelectrochemically etched current aperture

Ludovico Megalini<sup>\*1</sup>, Renuka Shenoy<sup>2</sup>, Kenneth Rose<sup>2</sup>, James P. Speck<sup>1</sup>, John E. Bowers<sup>1,2</sup>, Shuji Nakamura<sup>1,2</sup>, Daniel A. Cohen<sup>1</sup>, and Steven P. DenBaars<sup>1,2</sup>

<sup>1</sup> Department of Materials, University of California, Santa Barbara, CA 93106, USA

<sup>2</sup> Department of Electrical and Computer Engineering, University of California, Santa Barbara, CA 93106, USA

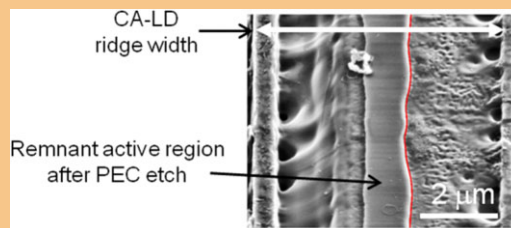
Received 28 July 2015, revised 29 November 2015, accepted 21 December 2015

Published online 26 January 2016

**Keywords** focused ion beam, InGaN, laser diodes, light scattering, photoelectrochemical etching, roughness

\* Corresponding author: e-mail megalini@engineering.ucsb.edu, Phone: +1-805-689-0211, Fax: +1-805-893-8983

We estimate the roughening-induced scattering optical losses in III-nitride current aperture laser diodes (CA-LDs) caused by imperfect photoelectrochemical (PEC) etching of the active region of a (2021) InGaN multi quantum well (MQW) laser diode. Roughness data were obtained by atomic force microscope (AFM) and scanning electron microscope (SEM) image processing of the remnant PEC-etched waveguides after the top p-layers were removed by focused ion beam cuts. Roughness (correlation length) values of  $\sim 60$  ( $\sim 600$ ) nm have been measured that cause optical loss in the range of  $\sim 8$  cm<sup>-1</sup> as estimated by using the 3D volume current method (VCM). Larger and more irregular bends contribute more significantly to the scattering loss.



Extraction of the roughness (red line) from one edge of the remnant photoelectrochemical (PEC) etched active region of current aperture laser diode (CA-LD) by image processing after the p-epilayers were removed by focused ion beam (FIB).

© 2016 WILEY-VCH Verlag GmbH & Co. KGaA, Weinheim

**1 Introduction** Theoretical and experimental analysis have shown that constricting the current to flow to the center of the lasing mode by laterally and controllably etching the active region can improve the performance of optoelectronic [1] and electronic [2] devices by eliminating current leakage pathways and reducing the attendant dc-rf dispersion. Selective wet etching of an InGaAsP active layer from a InP-based structure has been used to undercut the active region and achieve low-threshold and high-speed devices [3].

The III-nitrides lack conventional wet etchants [4] and instead rely mainly on chlorine-based dry etching methods which do not allow any controllable undercut in the lateral direction and produce sub-surface damage to the epitaxial structure. Dry etch damage can reduce the performance,

reliability, and lifetime of the final devices. In addition, dry etching can induce high surface roughness, which is generally correlated to corrugations of the photoresist profile and to the etch rate [5] between the waveguide core and the outer cladding. This is undesirable in optoelectronics devices, especially in the case of high-index-contrast (HIC) optical devices.

By contrast, wet etching usually causes less damage and produces smoother surfaces. Photoelectrochemical (PEC) etching has emerged as a promising wet etching technique for nitride-based materials, having already been applied successfully to Si and other III–V compounds [6]. By PEC etching the active region, CW operation of a III-N current aperture laser diode (CA-LD) [7] and a current aperture vertical electron transistor [8] (CA-VET) have been demonstrated.

Here we estimate the scattering modal losses caused by the PEC etch-induced roughness of the active region of nitride-based CA-LD fabricated as described in Ref. [7]. We suggest possible ways to mitigate these scattering losses and, therefore, improve the differential efficiency of the final device.

**2 Estimation of roughness-induced scattering loss in PEC etched LD** Scattering losses are caused by the forward- and backscattered radiated power of the guided optical mode [9–11], whose shape changes continuously along the light propagation direction because of the continuous change of the beta of the optical mode,  $\beta = k_0 \cdot n_{\text{eff}}$  due to the sidewall roughness [12–15], where  $k_0$  represents the free wavelength wavevector and  $n_{\text{eff}}$  the effective index of the entire LD structure [16]. This is usually assumed to occur only along the edge (line edge roughness, LER), and it is modeled as a zero-mean real function  $f(z)$  as depicted in Fig. 1.

According to the volume current method [17] (VCM), a rough waveguide is modeled as a perfectly smooth and straight waveguide, which does not contribute to the far field radiation, associated with a polarization current distribution [18]  $\vec{J}(\vec{r})$  representing the refractive index inhomogeneity at the rough edges:

$$\vec{J}(\vec{r}) = -i \frac{2\pi}{\lambda} \epsilon_0 \cdot \Delta n_{\text{eff}}(x) \cdot \vec{E}_{\text{pol}}(x, y) \delta(y) \delta(z), \quad (1)$$

where  $\lambda$  is the light propagating wavelength,  $i$  is imaginary unit,  $\epsilon_0$  is the vacuum permittivity,  $\delta$  is the Dirac delta function,  $\vec{E}_{\text{pol}}(x, y)$  is the electric field, and  $\Delta n_{\text{eff}}(x)$  is difference between the square of core and cladding effective refractive index.  $\vec{E}_{\text{pol}}(x, y)$  is assumed to be very similar to that of the perfectly smooth and straight waveguide, and it contains the information on the TE (or TM) polarization of the waveguide. In the CA-LD design, this translates to the difference between the effective refractive index of the unetched active region and the PEC etched aperture region, respectively:

$$\Delta n_{\text{eff}}(x) \equiv n_{\text{eff, unetched}}^2 - n_{\text{eff, aperture}}^2(x). \quad (2)$$

Typically  $\Delta n_{\text{eff}}(x)$  is a step function but, in general, the index profile can be distributed, i.e., in CA-LD design it can take into account the tapered shape of the aperture, which is

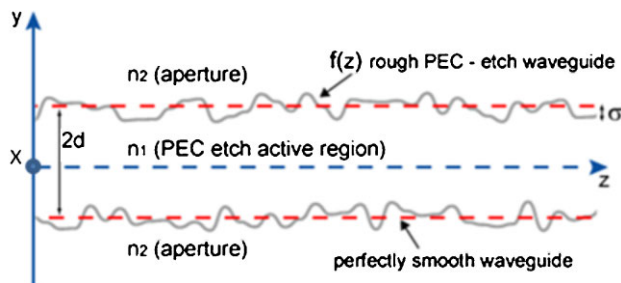


Figure 1 Schematics of LER in the CA-LD.

related to the different polarization fields of the crystal planes.

In order to apply the VCM to the CA-LD we modeled it in FIMMWAVE, a commercially available 2D waveguide mode solver. The total LD ridge width is  $4.8 \mu\text{m}$  and its active region (4 MQW, 3.5 nm QW and 6 nm barrier, the first barrier is 21 nm thick) is  $1.15 \mu\text{m}$  wide. The calculated confinement factor is  $\sim 4\%$ . We decomposed the structure in three layers [19] and we estimated to the first order the effective refractive index of the slice containing the aperture as

$$n_{\text{eff, aperture}} \approx \Gamma_{\text{aperture}} \cdot n_{\text{air}} + (1 - \Gamma_{\text{aperture}}) \cdot n_{\text{eff, unetched}}, \quad (3)$$

where  $\Gamma$  is the optical mode confinement factor,  $n_{\text{eff, unetched}}$  and  $n_{\text{air}}$  are the refractive index of the un-etched region and air, respectively. As a result, FIMM wave simulations indicate that a CA-LD can be considered similar to a deeply etched ridge LD placed in an environment of refractive index equal to 2.406 as shown in Fig. 2. The two structures have the same beta, whereas the difference in the confinement factor is

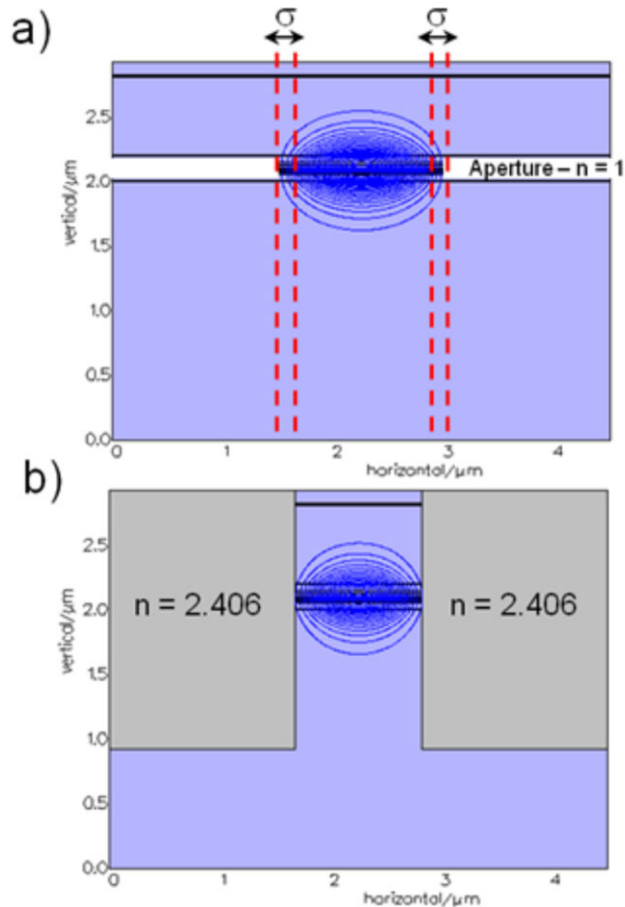


Figure 2 Simulation of the electric field intensity for (a) the CA-LD and (b) deep etched ridge LD.  $\sigma$  indicates the total waveguide roughness, i.e., the deviation from the perfectly smooth and straight waveguide.

0.1%. The step effective index between the unetched and PEC-etched region is estimated to be  $\Delta n_{\text{eff}}(x) \approx 0.074$ .

The far field radiation pattern in 3D can be obtained as the product of a finite height radiating element whose height corresponds to the PEC-etched MQW thickness and an array factor representing its distribution along the waveguide. In this way, both the finite dimensions and the polarization of the actual waveguide are taken into account and a more precise estimation [19] of the scattering losses can be obtained compared to the 2D model [20]. In particular, the radiated power is proportional to the product of the Poynting vector of the polarization current source produced by the refractive index inhomogeneity along the light propagation direction, the line edge roughness power spectral density function (PSD), which is related to the autocorrelation function (ACF) by the Wiener–Khinchine theorem [21] and the difference in effective refractive indices the core-cladding squared  $\Delta n_{\text{eff}}^2(x)$  and inversely proportional to the emission wavelength of the device.

### 3 Experimental

**3.1 Estimation of the roughness of the remnant PEC etched active region** Roughness values of the PEC etched active region edges were previously obtained by analysis of fluorescence optical microscope images [22]. Although optical microscope images can provide very large dataset, which is necessary to have a good estimation of the parameters to be measured [23], they suffer from low resolution in analyzing very small features. More precise measurements of the remnant PEC etched active region edges features have been obtained by high resolution AFM and SEM images analysis (a pixel on the SEM image corresponds to  $\sim 3$  nm, the SEM resolution is  $\sim 1.2$  nm) after removing the p-layers using a FEI Helios 600 dual focused ion beam (FIB). In order to reduce scalloping caused by the physical sputtering of the FIB and to avoid additional damage, the cuts were performed in multiple steps with the ion beam operating in rastering mode at 30 keV, and the beam current was varied from 0.46 nA down to 28 pA. The SEM images were recorded at 0.34 and 0.69 nA electron beam currents to increase the contrast of the rough edge to the background gray, using dwell times of 3 and 10  $\mu\text{s}$  to enhance the signal-to-noise ratio and avoid distortion. By carefully monitoring the ion milling through the different layers of the structures during the cut, this was stopped exactly on the top of the remnant PEC-etched active region as shown in Fig. 3.

We performed statistical analysis on the rough edges after extracting them by using a modified hidden Markov model (HMM)-based algorithm [24]. The trellis was created by initializing a roughly estimated vertical line, constructing normal lines at each pixel along this line, and symmetrically sampling points on each normal. Observation probabilities of the HMM were designed to favor sharp edges and transition probabilities to ensure a smooth-connected edge. Dynamic programming was applied to estimate the HMM state

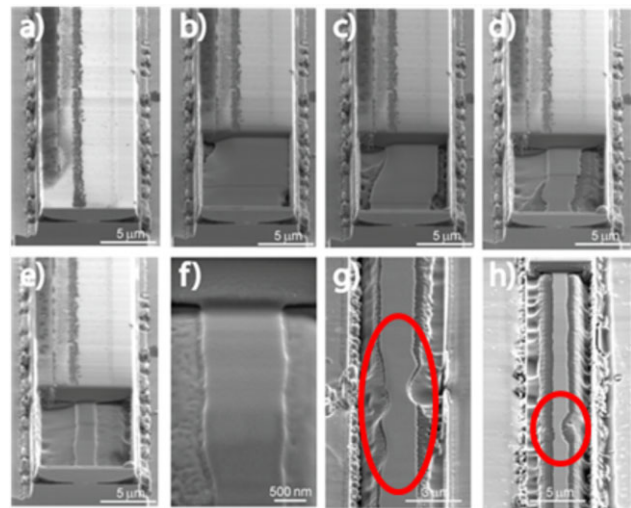


**Figure 3** FIB cuts of the p-epilayers of a CA-LD exposing the remnant PEC etched active region. Images (a)–(h) show SEM images recorded at 52°, (g) and (h) at 90°. Circles indicate region of very wide bends. Scale bar is 5  $\mu\text{m}$  ((image (a)–(e) and (h)), 500 nm (image (f)), and 3  $\mu\text{m}$  (image (g)).

sequence having maximum *a posteriori* probability, and hence, the optimal edge position [24]. The result is shown in Fig. 4(a)–(b). A similar procedure has been applied to AFM scan images (Fig. 4(a)). The roughness data obtained from the SEM images are on the same order of magnitude of those obtained by AFM images on a smaller scan.

**4 Results and discussion** The correlation length  $L_c$  of the rough sidewalls was obtained by computing the point where the autocorrelation function  $\mathcal{R}_x(z)$  of the edge

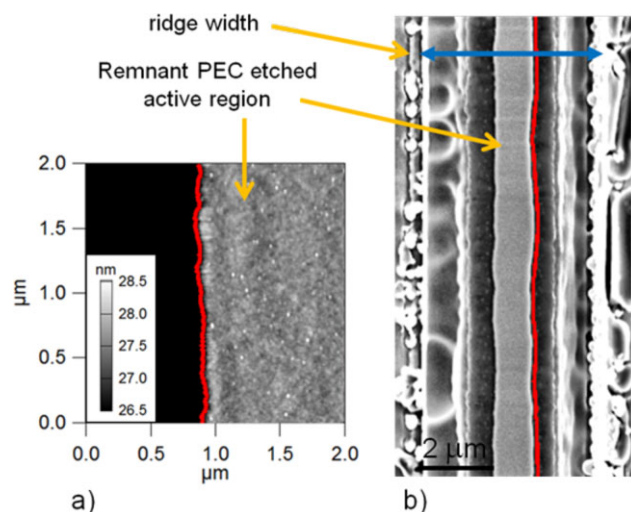


**Figure 4** Roughness extraction of the remnant PEC etched active region edges of CA by image processing: (a) an AFM image, (b) a SEM image.

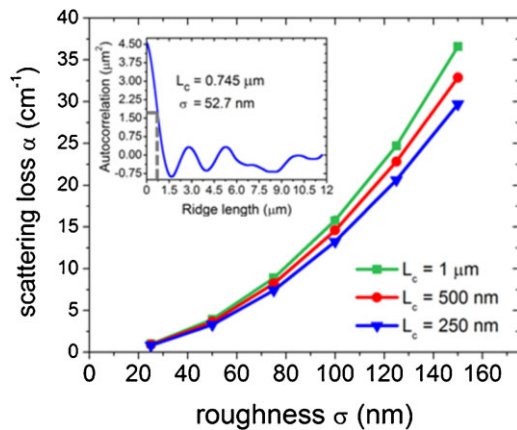


**Figure 5** Plot of scattering loss vs. roughness for different correlation lengths  $L_c$ . Inset: autocorrelation function of the roughness of a CA-LD.

roughness  $f(z)$  decays to  $e^{-1}$  of its maximum:

$$\mathcal{R}_x(L_c) = e^{-1} \cdot \int_{-\infty}^{\infty} x(z) \cdot x(z + \delta) dz. \quad (4)$$

Figure 5 shows a plot of loss vs. roughness standard deviation ( $\sigma$ ) for different correlation lengths. As expected the losses increase as  $\sigma$  increases. A decrease in  $L_c$  leads to a decrease in the scattering losses because a shorter  $L_c$  indicates an increase in the higher-frequency component of the roughness PSD, and usually scattering losses are mainly caused by low frequency component corresponding to a slower and wider variations in the remnant active region width.

The range for  $L_c$  and the roughness measured is in the order of  $\sim 600 \pm 150$  nm and  $\sim 60 \pm 20$  nm, respectively. This will cause optical scattering losses estimated in the range  $\sim 8\text{--}10$  cm $^{-1}$  for the CA-LD of Ref. [7]. Although relatively high, this value is consistent with other propagation losses of GaN based waveguides reported in the literature [25, 26].

The roughness-induced scattering loss computation so far presented does not take into account the very irregular and wide bends like those shown in Fig. 3(g) and (h). Simulations done in FIMMPROP, a 3D beam propagation commercial software, indicate that adiabatic change of a perfectly smooth active region width does not contribute significantly to the radiation loss (Fig. 6(a)) and  $\sim 99\%$  of the optical power is transmitted (Fig. 6(b)). By contrast, if the remnant PEC-etched active region has an extremely irregular shape (Fig. 3(g) and (h)) the optical losses can be more significant: simulations suggest that only a fraction of the power can be transmitted. Further analysis is ongoing. In general, if extended defects are not present in the structure, roughness can be greatly reduced by optimization of the fabrication process parameters. In the case of PEC etching, this can be carried out by choosing the best PEC etch

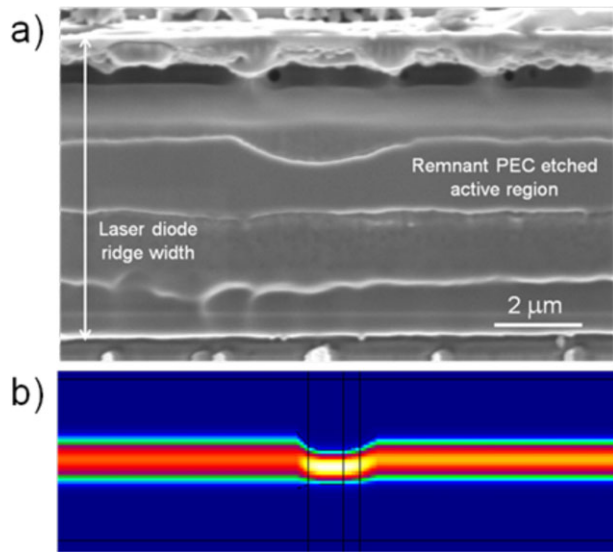


**Figure 6** (a) PEC etched active region of a CA-LD having a tapered shape. (b) Corresponding profile of the electric field intensity.

conditions in terms of light intensity, molarity concentration of the electrolyte and stirring speed of the solution. Optimized epitaxial structure on high quality bulk GaN substrates is also essential to obtain smooth PEC etch as this depends on uniform carrier lifetime. Extended defects such as threading and misfit dislocations provide sites for non-radiative carrier recombination and thus they slow or halt the etching. Finally, Eqs. (1) and (2) suggest that reducing the refractive index step between the unetched active region and the aperture PEC-etched region, for example by filling the airgap with polymer or oxide, can also help to decrease the scattering loss.

**5 Conclusion** In this paper, we estimated the scattering optical losses in nitride current aperture laser diodes (CA-LDs) in which the aperture was fabricated by selective photoelectrochemical (PEC) etching the active region of a (20 $\bar{2}$ 1) LD structure. The roughness-induced optical losses were estimated using a 3D volume current model in conjunction with roughness data obtained by AFM and SEM images processing of the remnant PEC-etched active region. PEC etch process optimization (in particular the solution molarity, stirring and temperature, the light source, and intensity) and advanced fabrication techniques (for example, by filling the airgap to reduce the refractive index step between the PEC-etched and the un-etched active region) can reduce these scattering losses while maintaining the benefits of the current aperture, therefore, increasing overall the devices performance.

**Acknowledgements** The authors would like to thank Dr. D. John and Dr. J. Bauters for sharing the VCM code to compute the 3D scattering loss. This work was supported by the Solid State Lighting and Energy Center (SSLEEC) at UCSB. A portion of this work was done in the UCSB nanofabrication

facility, part of the NSF NNIN network (ECS-0335765), as well as the UCSB MRL, which is supported by the NSF MRSEC program (DMR1121053).

## References

- [1] J. E. Bowers, B. R. Hemenway, A. H. Gnauck, T. J. Bridges, E. G. Burkhardt, D. P. Wilt, and S. Maynard, *Appl. Phys. Lett.* **47**, 78 (1985).
- [2] S. Chowdhury, M. H. Wong, B. L. Swenson, and U. K. Mishra, *IEEE Electron Device Lett.* **33**, 41 (2012).
- [3] M. M. Dummer, J. R. Raring, J. Klamkin, A. Tauke-Pedretti, and L. A. Coldren, *Opt. Express* **16**, 20388 (2008).
- [4] D. Zhuang and J. H. Edgar, *Mater. Sci. Eng. R* **48**, 1 (2005).
- [5] K. Zhu, V. Kuryatkov, B. Borisov, J. Yun, G. Kipshidze, S. A. Nikishin, H. Temkin, D. Aurongzeb, and M. Holtz, *J. Appl. Phys.* **95**, 4635 (2004).
- [6] P. A. Kohl, *IBM J. Res. Developm.* **42**, 629 (1998).
- [7] L. Megalini, D. L. Becerra, R. M. Farrell, A. Pourhashemi, J. S. Speckl, Shuji Nakamura, S. P. DenBaars, and D. A. Cohen, *Appl. Phys. Express* **8**, 042701 (2015).
- [8] Y. Gao, I. Ben-Yaacov, U. K. Mishra, and E. L. Hu, *J. Appl. Phys.* **96**, 6925 (2004).
- [9] D. Marcuse, *Bell Syst. Tech. J.* **48**, 3187 (1969).
- [10] P. K. Tien, *Appl. Opt.* **10**, 2395 (1971).
- [11] M. Kuznetsov and H. A. Haus, *IEEE J. Quantum Electron.* **19**(10), 1505 (1983).
- [12] F. Toor, D. L. Sivco, H. E. Liu, and C. F. Gmachl, *Appl. Phys. Lett.* **93**, 031104 (2008).
- [13] J. F. Bauters, M. J. R. Heck, D. John, D. Dai, M. C. Tien, J. S. Barton, A. Leinse, R. G. Heideman, D. J. Blumenthal, and J. E. Bowers, *Opt. Express* **19**(4), 3163 (2011).
- [14] J. Shin, Y. Chang, and N. Dagli, *Opt. Express* **17**(5), 3390 (2009).
- [15] K. K. Lee, D. R. Lim, H. C. Luan, A. Agarwal, J. Foresi, and L. C. Kimerling, *Appl. Phys. Lett.* **77**, 1617 (2000).
- [16] L. A. Coldren, S. W. Corzine, and M. Mashanovic, *Diode Lasers and Photonic Integrated Circuits*, 2nd edn. (Wiley, New York, 2012).
- [17] A. W. Snyder and J. D. Love, *Optical Waveguide Theory* (Chapman & Hall, London, 1983).
- [18] T. Barwicz, and H. Haus, *J. Lightwave Technol.* **23**, 2719 (2005).
- [19] C. Ciminelli, V. M. N. Passaro, F. Dell'Olio, and M. N. Armenise, *J. Europ. Opt. Soc. Rapid Pub.* **4**, 09015 (2009).
- [20] F. P. Payne and J. P. Lacey, *Opt. Quantum Electron.* **26**, 977–986 (1994).
- [20] F. P. Payne and J. P. Lacey, *Opt. Quantum Electron.* **26**, 977–986 (1994).
- [21] F. Ladouceur, J. D. Love, and T. J. Senden, *IEE Proc.: Optoelectron.* **14**, 242 (1994).
- [22] L. Megalini, L. Y. Kuritzky, J. T. Leonard, R. Shenoy, K. Rose, S. Nakamura, J. S. Speck, D. A. Cohen, and S. P. DenBaars, *Appl. Phys. Express* **8**, 066502 (2015).
- [23] J. A. Ogilvy and J. R. Foster, *J. Phys. D: Appl. Phys.* **22**, 1243 (1989).
- [24] M. E. Sargin, A. Altinok, B. S. Manjunath, and K. Rose, *IEEE Trans. Image Process.* **20**, 1023 (2011).
- [25] A. Lupu, F. H. Julien, S. Golka, G. Pozzovivo, G. Strasser, E. Baumann, F. Giorgetta, D. Hofstetter, S. Nicolay, M. Mosca, E. Feltn, J. F. Carlin, and N. Grandjean, *Photon. Technol. Lett.* **20**, 102 (2008).
- [26] Y. Li, A. Bhattacharyya, C. Thomidis, T. D. Moustakas, and R. Paiella, *Opt. Express* **15**, 5860 (2007).